1st Spanish Fluid Mechanics Conference
Cádiz, June 19-22, 2022

Aerodynamic Study of the NASA's X-43A Hypersonic Aircraft

Àlex Navó[1,*] and Josep M Bergada[1,†]

[1] *Department of Fluid Mechanics, Universitat Politècnica de Catalunya, Barcelona, 08034, Spain*

A two-dimensional aerodynamic study of the NASA's X-43A hypersonic aircraft is developed using two different approaches. The first one is analytical and based on the resolution of the oblique shock wave and Prandtl–Meyer expansion wave theories supported by an in-house program and considering a simplified aircraft's design. The second approach involves the use of a Computational Fluid Dynamics (CFD) package, OpenFOAM and the real shape of the aircraft. The aerodynamic characteristics defined as the lift and drag coefficients, the aerodynamic efficiency and the pitching moment coefficient are calculated for different angles of attack. Evaluations are made for an incident Mach number of 7 and an altitude of 30 km. The CFD approach has been extended to a full three-dimensional model in order to be compared with the 2D model.

INTRODUCTION

NASA X-43A, also known as a Hyper-X Research Vehicle (HXRV), was one of the different NASA's uncrewed hypersonic aircraft designed with the innovative scramjet propulsion technology to fly at high speeds and high altitudes. Hyper-X was also the experimental hypersonic flight research program of X-43A managed by NASA whose main objective was to demonstrate, validate and implement the technology, the experimental techniques and the computational methods and tools for design and performance predictions of a hypersonic aircraft with an airframe-integrated, scramjet propulsion system. In order to obtain the required data, NASA designed and fabricated three similar X-43A vehicles; two of them were designed to fly at Mach 7 and the other one at Mach 10. All of them measured around 3.66 m in length and weighted roughly 1361 kg.

Among the first studies undertaken on such hypersonic flight vehicles, it is interesting to highlight the three-dimensional inviscid CFD results in support of the Hyper-X vehicle aerodynamic database presented in [1]. The pressure distribution over this particular aircraft was numerically determined in [2], where an algorithm based on the quasi-gas dynamic system of equations was created with the objective of introducing artificial dissipation coefficients. The level lines of density and streamlines in the computational domain were also illustrated, in which a vortex at the trailing edge of the aircraft was identified. The lift and drag coefficients and the lift–drag ratio for several angles of attack by solving the three-dimensional Navier–Stokes equations were presented in [3, 4]. The comparison between these parameters and different experimental measurements gave a relatively good agreement. One of the latest CFD studies on the NASA's X-43A hypersonic aircraft was performed by [5], where several configurations of a simplified two-dimensional model was analysed.

RESULTS

The geometry of the simplified X-43A is defined by the design angles α_1, α_2, α_3 and α_4 and $x_1 = 3.66$ m, $x_{23} = 1.83$ m, $Y = 0.2225$ m, $x_4 = 0.762$ m and $x_5 = 1.068$ m. In this case, the scramjet is neglected. All these features are presented in Figure 1 where, for this particular angle of attack, two oblique shock waves with associated angles (β_2 and β_3) appear at the beginning of stages 2 and 3 and three Prandtl–Meyer expansion waves at the beginning of stages 1, 4 and 5. Moreover, θ_1 and θ_2 are characterising the deflection angles between the unperturbed flow given by M_∞ and stages 1 and 2.

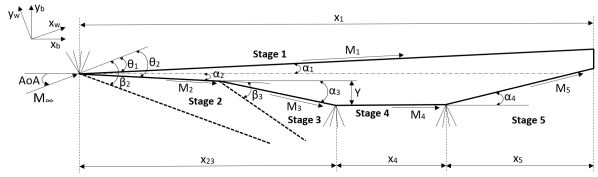

FIG. 1. Oblique shock waves and Prandtl–Meyer expansion waves on the simplified shape of X-43A.

The main characteristics of the three different cases considered for the 2D CFD study are shown in Table I.

TABLE I. Design angles values of the three CFD cases.

Case	Design Angles			
	α_1 (°)	α_2 (°)	α_3 (°)	α_4 (°)
1	2.7	3.07	11.5	13.9
2	1	3.07	10.8	10
3	0	2	12.2	11.8

Case 1 is presented with the variation of the pressure field throughout the aircraft at a zero angle of attack in Figure 2a. Since the angle of attack, AoA, is smaller than α_1, a shock wave is produced at the beginning of the extrados where, consequently, the pressure is increased and remains approximately constant along the surface. This phenomenon is also present in the aircraft nose (stages 2 and 3); in case of stage 3, the increase of pressure is more significant due to the difference in the design angles ($\alpha_3 >> \alpha_1$ & α_2, see Table I).

Figure 2b shows that shock waves of stages 1 and 2 are completely attached to the sharp leading edge of the wedge. X-43A uses the fuselage nose part to form the shock in front of the intake. Theoretically (according to the analytical model), the aircraft should fly with the nose optimised configuration under those conditions of

design angles and AoA. Such configuration is produced when both oblique shock waves produced at the nose focus in the tip of the scramjet. Focusing on Figure 2c, shock 2 (which is the one formed at the beginning of stage 2) is focused on the tip of the lower edge, while shock 3 (the one that corresponds to the shock wave created at the beginning of stage 3) is slightly deflected into the entrance of the throat.

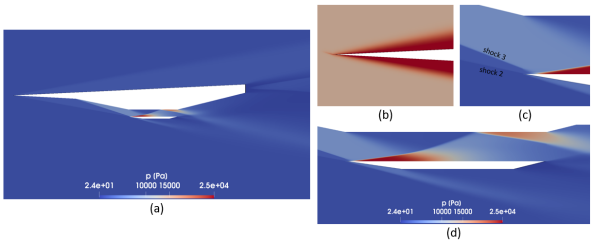

FIG. 2. Pressure field of case 1 for $AoA = 0°$, (**a**) all the aircraft, (**b**) attached leading edge (different colour scale), (**c**) tip of the lower edge of the scramjet, (**d**) scramjet region.

Inside the scramjet, different things occur together (see Figure 2d for more detail). On the one hand, the flow expands as a Prandtl–Meyer expansion wave being produced at the end of stage 3. As a result, there is a small region situated in the upper left side in which the pressure decreases from that of the previous stage. On the other hand, shock 3 reflects from the lower edge generating a new shock, which, in turn, reflects from the upper edge forming, once again, another shock wave. In other words, two regular reflections in steady flow inside the engine are created. The first reflection leads to a high pressure region downstream at about 25 kPa, while the pressure after the second reflection is 15 kPa approximately. This phenomenon is known as the shock diamond and provides some regions with strong adverse pressure gradients which induce flow separation. Finally, at the end of the upper right side of the scramjet, a Prandtl–Meyer expansion wave is originated. The pressure decreases and remains constant along the surface all the way to the trailing edge.

The lift coefficient, C_L, drag coefficient, C_D, aerodynamic efficiency, E, and pitching moment coefficient, $C_{M_{CG}}$, in terms of the AoA for the three CFD cases, are shown in Figure 3. As seen in Figure 3a, case 3 has the highest lift coefficient until $AoA = 6°$. According to Figure 3b, case 1 has the highest drag coefficient up to $AoA = 2°$, where the first place is replaced by case 3, and case 1 has a very similar drag coefficient as case 2. Both cases 2 and 3 have a similar E according to Figure 3c; the aerodynamic efficiency of case 3 is higher for $AoA = [-4, -2, 0, 2]°$ and lower for the other angles of attack. Therefore, the maximum aerodynamic efficiency of case 2 is the highest one ($E_{max} = 3.52$ for $AoA = 6°$). In addition, from $AoA = 10°$, all cases seem to converge to a certain value. Finally, the behaviour of the pitching moment coefficient through the different angles indicates a longitudinal instability condition with regard to any perturbation of the AoA (Figure 3d); cases 1 and 2 are mostly similar according to this graph, while case 3 has the highest pitching moment coefficient for $AoA = [-4, -2, 0]°$ and the lowest one for the other angles of attack.

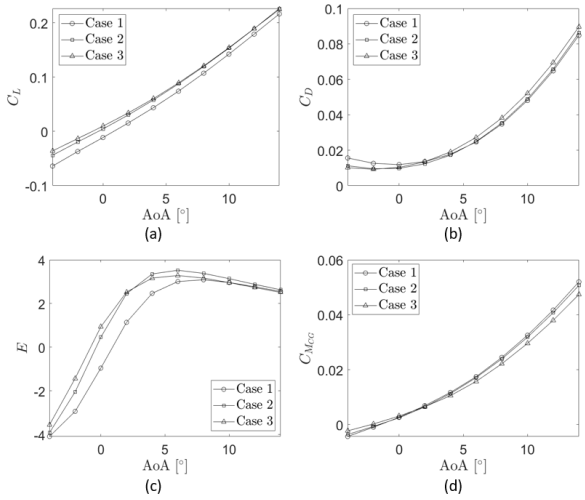

FIG. 3. Aerodynamic parameters in terms of the angle of attack of the three CFD cases, (**a**) C_L vs. AoA, (**b**) C_D vs. AoA, (**c**) E vs. AoA, (**d**) $C_{M_{CG}}$ vs. AoA.

Finally, the 3D CFD study is currently being developed and will be presented in the conference.

CONCLUSIONS

From the three CFD cases studied, cases 2 and 3 present a similar aerodynamic performance, while case 1 is worse in such aspect. Furthermore, oblique shock waves and Prandtl-Mayer expansion waves along with other flow phenomena could have been visualised at such hypersonic flow conditions.

* alexnavopinyol@gmail.com
† josep.m.bergada@upc.edu

[1] A. Frendi, On the cfd support for the hyper-x aerodynamic database, in *37th Aerospace Sciences Meeting and Exhibit* (1999) p. 885.
[2] T. Elizarova and I. Shirokov, Artificial dissipation coefficients in regularized equations of supersonic aerodynamics, in *Doklady Mathematics*, Vol. 98 (Springer, 2018) pp. 648–651.
[3] A. Zheleznyakova and S. T. Surzhikov, Application of the method of splitting by physical processes for the computation of a hypersonic flow over an aircraft model of complex configuration, High Temperature **51**, 816 (2013).
[4] A. Zheleznyakova and S. T. Surzhikov, Calculation of a hypersonic flow over bodies of complex configuration on unstructured tetrahedral meshes using the ausm scheme, High temperature **52**, 271 (2014).
[5] À. Navó and J. M. Bergada, Aerodynamic study of the nasa's x-43a hypersonic aircraft, Applied Sciences **10**, 8211 (2020).